Editors' Suggestion | Featured in Physics

Position Measurement of a Levitated Nanoparticle via Interference with Its Mirror Image

Lorenzo Dania,[1,*] Katharina Heidegger,[1] Dmitry S. Bykov,[1] Giovanni Cerchiari,[1] Gabriel Araneda,[2] and Tracy E. Northup[1]

[1]*Institut für Experimentalphysik, Universität Innsbruck, Technikerstraße 25, 6020 Innsbruck, Austria*

[2]*Department of Physics, Clarendon Laboratory, University of Oxford, Parks Road, Oxford OX1 3PU, United Kingdom*

(Received 3 January 2022; accepted 20 May 2022; published 28 June 2022)

Interferometric methods for detecting the motion of a levitated nanoparticle provide a route to the quantum ground state, but such methods are currently limited by mode mismatch between the reference beam and the dipolar field scattered by the particle. Here we demonstrate a self-interference method to detect the particle's motion that solves this problem. A Paul trap confines a charged dielectric nanoparticle in high vacuum, and a mirror retro-reflects the scattered light. We measure the particle's motion with a sensitivity of 1.7×10^{-12} m$/\sqrt{\text{Hz}}$, corresponding to a detection efficiency of 2.1%, with a numerical aperture of 0.18. As an application of this method, we cool the particle, via feedback, to temperatures below those achieved in the same setup using a standard position measurement.

DOI: 10.1103/PhysRevLett.129.013601

In state-of-the-art levitated optomechanics experiments, dipole radiation elastically scattered by a submicron particle is collected by a lens with high numerical aperture (NA) [1,2], and interference with a Gaussian reference beam enables reconstruction of the particle's motion [3,4]. The detection efficiency achievable with these techniques has two fundamental limits [3]: first, the particle radiation away from the lens aperture is not collected, and thus information about the particle's position is lost. Second, the dipole radiation wave front and polarization do not match the Gaussian beam profile, reducing the interferometric visibility and thus the position measurement sensitivity. Both the limited collection efficiency and the mode mismatch present a challenge for achieving quantum control of a levitated particle's motion. While optically levitated particles have been cooled to their motional ground state [1,2,5], the quantum regime has remained out of reach for particles confined in ion traps [6,7] and magnetic traps [8–10], in which optical access is limited by the trap geometry. These latter approaches are nevertheless of particular interest for quantum-mechanical experiments with macroscopic objects, as they offer an environment free of light-induced decoherence.

Remarkable collection efficiencies for both nanoparticle emitters and atomic ion fluorescence have been achieved with deep parabolic mirrors [11–13], but such setups are optimized for enhanced light-matter interaction rather than interferometric position detection. Near-ideal mode matching is obtained in experiments in which the dipolar emission is referenced to its mirror image via homodyne detection. For example, self-interference detection is exploited in trapped-ion experiments for detecting mechanical motion with sensitivities at the level of single quanta [14,15], and similar techniques are used in fluorescence microscopy [16,17] for determining the structure and diffusion of chemical components in biological tissue with subwavelength resolution [18]. Recently we argued that, compared to known methods, self-homodyne detection is the closest realization of a quantum-limited measurement for the position of a dipolar scatterer [19], but until now, this technique has not been adapted to a levitated optomechanics experiment, nor has its efficiency been compared experimentally to that obtained with other methods.

Here we report on the optical detection of the motion of a silica nanoparticle by self-interference, and we compare the detection efficiency with both a forward-detection technique implemented in parallel and ideal quantum-limited detection. Furthermore, we show that the position signal obtained with the self-homodyne method enables real-time feedback cooling of the particle's motion. In our proof-of-principle demonstration, the nanoparticle is trapped in a linear Paul trap under high vacuum, but the detection technique can be extended to setups that confine dipolar emitters by magnetic or optical forces.

The self-homodyne method allows us to measure the position of a nanosphere relative to a mirror. The essence of self-homodyne can be understood by considering a movable mirror, a detector, and a levitated particle illuminated by a laser beam of wavelength λ [Fig. 1(a)]. The particle is located between the mirror and the detector. Laser light scattered by the particle may impinge directly on the

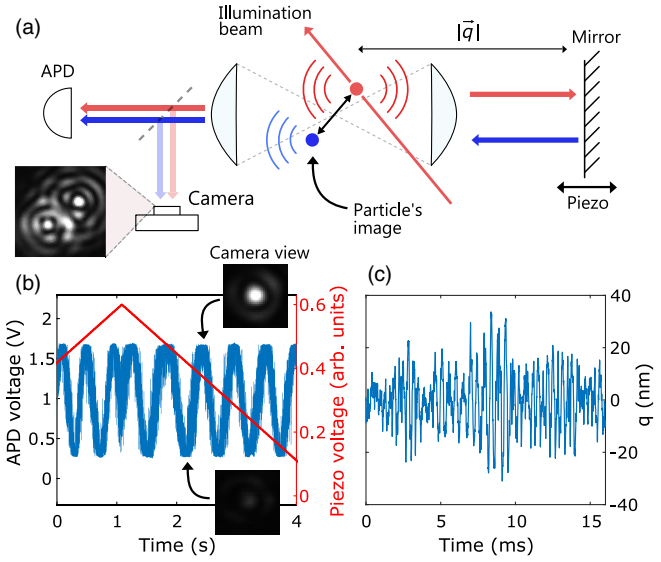

FIG. 1. Basic principles of the self-homodyne technique. (a) The particle is illuminated by a laser beam and two confocal lenses collect the scattered light. The image created by one lens is reflected back to the particle by a distant flat mirror. The reflected light interferes with the directly scattered light, and the other lens images the two fields on a detector. The phase of the interferometric signal measured by the detector depends on the mutual particle-mirror distance along the q axis. Inset shows a camera image of the nanoparticle and its mirror image. Here, for visualization purposes, the images are displaced from each other. (b) Typical detector output (blue) when the mirror is linearly displaced in time with a piezo translation stage. The driving ramp voltage of the mirror (red) occurs with a subhertz period. Insets show camera images obtained at maximum and minimum of the interferometric fringe, respectively. (c) Time trace of the particle's displacement q for the case of a fixed mirror position. Particle oscillations occur at frequencies of a few kilohertz.

detector, or it may be reflected first from the mirror and only afterward reach the detector. Here, we consider a planar mirror and a planar detector, so we also include two confocal lenses that collimate the scattered light. These two light fields—the one that is directly scattered and the one that is first reflected—interfere at the detector; the interference phase depends on the distance between particle and mirror [Fig. 1(b)] [20]. In contrast, if the mirror position is held fixed, one observes a signal proportional to the particle position [Fig. 1(c)].

We employ two different modes to control the mirror's position via a piezoelectric stage: either we actively stabilize the mirror's position in order to monitor the particle, or we apply a linear ramp to calibrate the amplitude of the particle's motion. In the first case, the mirror position is locked to a point at which the fringes in Fig. 1(b) have a maximum slope, so that we have both linear detection and the best sensitivity. The lock compensates for drifts in the mirror position; it is able to distinguish between changes in the mirror position and changes in the nanosphere's position because the former occur on timescales much longer than the nanosphere period of oscillation. Note that the lock will only work if the nanosphere's amplitude of motion Δq is below $\lambda/4$, that is, within the turning points of the error signal, and linear detection requires the stronger condition $\Delta q \ll \lambda/4$.

In the second case, when we are interested in calibrating the nanosphere's amplitude of motion along the axis q of Fig. 1(a), we ramp the voltage applied to the piezo and measure the signal $V(t)$ recorded by the detector. In the linear regime around the set point, for low values of the NA, we can convert $V(t)$ to a displacement $q(t)$ along $\hat{q}$ using the expression $q(t) = V(t)/S$, where $S = 4\pi A/\lambda$ is the maximum slope of the interference fringe and A is the fringe amplitude [21]. This conversion assumes that displacement of the mirror is equivalent to displacement of the particle, which is a good approximation for NA $\lesssim 0.6$, as derived and discussed in the Supplemental Material [22]. This calibration relies only on the wavelength of the illuminating field; in contrast to other calibration techniques [27], no prior knowledge is required of the particle's mass or charge, and the particle does not need to be in thermal equilibrium with the background gas. For the measurements described below, the calibration is performed under high vacuum.

Having examined the core components, we now consider the larger experimental apparatus [Fig. 2(a)]. The nanoparticle, a silica sphere 300 nm in diameter [28], is confined in a linear Paul trap [29] under pressures as low as 2×10^{-8} mbar. The trap drive frequency is $\nu_{\mathrm{drive}} = 11$ kHz, and the secular trap frequencies are $(\nu_x,\nu_y,\nu_z) = (2.1, 3.2, 1.1)$ kHz, where $\hat{z}$ is the trap axis. Self-homodyne detection is implemented with a 780 nm laser beam. The beam is polarized along the z axis and illuminates the nanoparticle in the direction perpendicular to the mirror-particle axis q; the beam waist at the trapping position is 0.29(1) mm. Because of the Paul trap geometry, the self-homodyne detection axis q intersects both the $\hat{x}$ and the $\hat{y}$ axes at $\theta = 45°$, enabling displacement detection along both axes with equal sensitivity. When a nanoparticle is loaded into the Paul trap, it has an amplitude of motion larger than an optical wavelength. To cool the particle into the regime in which self-homodyne detection operates, we implement an auxiliary detection scheme. A 987 nm laser beam is focused on the particle with a waist of 2.7(3) μm along the q axis; its polarization is perpendicular to the z axis. We detect forward-scattered light from this beam in a split detection scheme, which we refer to as forward detection [3,6]. Polarizing beam splitters are used to decouple the 780 and 987 nm detection paths. From the forward-detection signal, we generate an error signal that is used to cool the particle to the millikelvin regime via feedback along all three motional axes [6]. Both the feedback and minimization of excess micromotion localize the particle well below $\lambda/4$, enabling linear detection through self-homodyne.

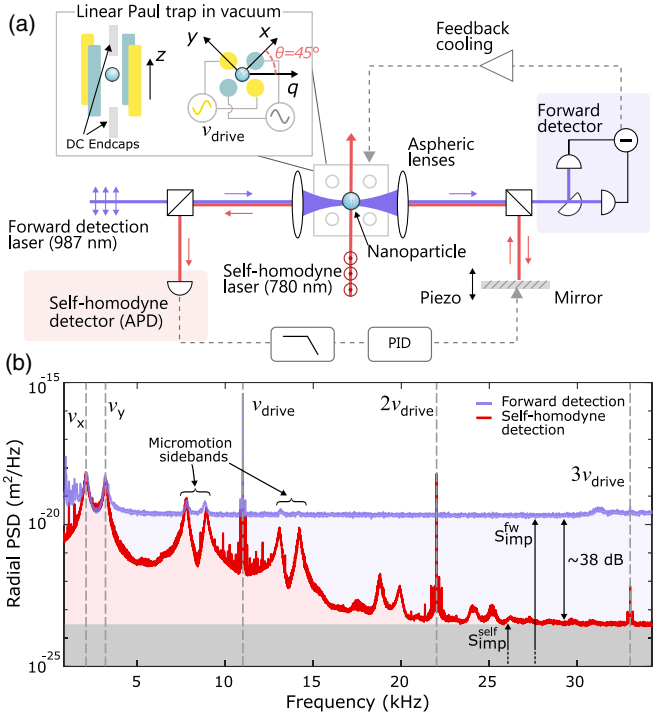

FIG. 2. Simultaneous self-homodyne and forward detection of a levitated nanoparticle. (a) Schematic overview of the setup. Lasers for the two detection methods are decoupled using polarization optics. For self-homodyne detection, the particle is illuminated with a weakly focused beam, and the particle's motion along the detection axis q is detected by an avalanche photodiode (APD). The APD signal is sent to feedback electronics consisting of a low-pass filter and a proportional–integral–derivative controller (PID) that stabilize the mirror position. For forward detection, light propagating along $\hat{q}$ is focused onto the particle and then guided, together with the forward-scattered light from the particle, to a set of balanced photodiodes. The light scattered by the particle from the two lasers is collected by a pair of aspheric lenses (NA = 0.18), which also focus and collimate the 987 nm beam. The inset shows the Paul trap axes. (b) Power spectral density (PSD) of the radial motion of one particle acquired simultaneously with the forward-detection method (purple) and with the self-homodyne method (red). Dashed gray lines indicate the trap radial frequencies ν_x and ν_y, the Paul trap's drive frequency ν_{drive}, and the first two harmonics of ν_{drive}. The measurement imprecisions $S_{\mathrm{imp}}^{\mathrm{self}}$ and $S_{\mathrm{imp}}^{\mathrm{fw}}$ are indicated.

Implementing forward detection allows us not only to cool the particle but also to compare the detection efficiencies of the two methods. For this comparison, two spectra are acquired simultaneously with the same particle. By fitting the calibrated self-homodyne spectrum with a Lorentzian, we extract the particle's temperature, which we use as a calibration for the spectrum obtained with the forward-detection method.

In Fig. 2(b), we plot the motional spectra acquired with the self-homodyne and forward-detection techniques. The two spectra have overlapping peaks at several frequencies that correspond to resonant motion of the particle. However, the noise floor of the self-homodyne spectrum is 38 dB below that of the forward-detection spectrum, and the new method resolves motional peaks that were hidden below the forward-detection noise floor. The noise floor of a calibrated motional spectrum corresponds to the measurement imprecision [30]; the imprecision of the self-homodyne measurement is $3.0(1) \times 10^{-24}$ m^2/Hz. The square root of this value corresponds to the motional sensitivity. From calculations based on [19], we expect the ratio of the measurement imprecision for the two cases to be 26 dB for identical detection conditions. Taking into account the different powers and losses in the two optical paths, we predict a ratio of 32 dB. We attribute the additional 6 dB to the particle not being centered in the focus of the forward beam [6].

Recently, measurement-based feedback cooling of nanoparticles to the motional ground state has been achieved in high-NA optical traps via detection of backward-scattered light [1,2]. The backward-detection technique is more efficient than forward detection, but nevertheless, from calculations based on Refs. [3,19] at our working NA of 0.18, we expect the self-homodyne imprecision to be 0.58 times smaller than that achieved with backward detection. We refer to Ref. [19] for a detailed comparison of the three methods.

We now turn our attention to how our implementation of self-homodyne detection compares to an ideal detection scenario. First, we characterize how the calibrated self-homodyne spectra depend on the scattered power over the full solid angle P, which is tuned by adjusting the self-homodyne beam power. As this power is varied, we correct for particle displacements induced by radiation pressure forces by applying electric fields in order to preserve optical alignment. For each value of P, we calibrate the motional spectrum by scanning the self-homodyne mirror. The calibrated spectra are shown in Fig. 3(a); we see in Fig. 3(b) that the spectra overlap at the particle's mechanical frequency and in Fig. 3(c) that each spectrum approaches a unique noise floor at high frequencies. Imperfect correction of particle displacements leads to slight variations of peak heights and frequencies in Fig. 3(b), due to the position-dependent cooling efficiency and gradient force, respectively.

The data of Fig. 3 show that increasing the power in the measurement field reduces the detection imprecision, as expected. Increasing the power does not, however, shift the mechanical resonance shown in Fig. 3(b), which tells us that the role of the gradient force is negligible, consistent with the fact that the self-homodyne beam is nearly collimated. We also see in Fig. 3(b) that the resonant peak height remains constant, from which we deduce that radiation-pressure shot noise is not heating the particle [31] and thus that backaction plays a negligible role at these laser powers and this background-gas pressure, as expected from calculations based on our system parameters [22].

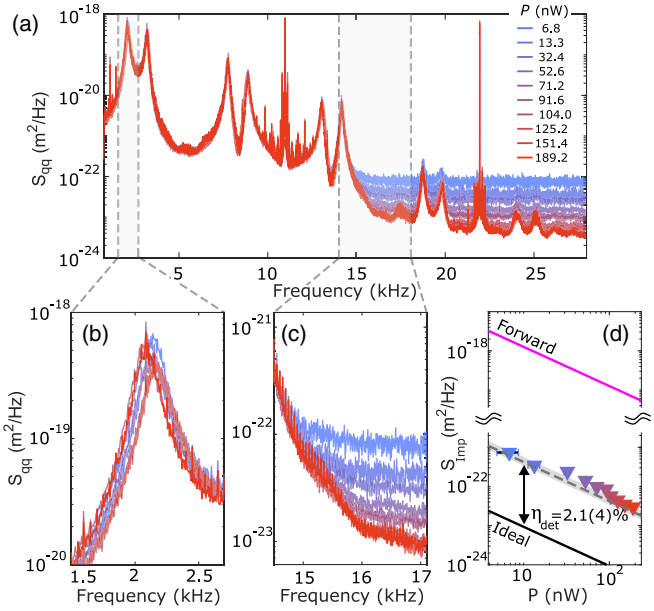

FIG. 3. Motional spectra acquired with self-homodyne detection for different values of the total scattered power P and with the same trapped particle. (a) Spectra over a frequency range that includes all detected mechanical resonances. (b) Closer view of the first radial resonance. (c) Closer view of the noise floor separation. Lower values of the noise floor are reached for higher values of the scattered power. Gain-dependent excess noise is subtracted. (d) Imprecision S_{imp} of self-homodyne detection as a function of the scattered power P of the particle, plotted as triangles. Error bars correspond to the uncertainty in the NA estimation. The black solid line indicates the expected imprecision for ideal detection [19] and the purple solid line indicates the imprecision for the forward detection inferred from our measurements. The gray dashed line and area represent the theoretically expected imprecision and its uncertainty, respectively. The distance between the black and gray lines is the detection efficiency η_{det}.

With these results in hand, we are now able to make a comparison with ideal detection. The detection imprecision is calculated as [19]

$$S_{\mathrm{imp}} = \frac{5\hbar c\lambda}{8\pi\eta_{\mathrm{det}}P}, \tag{1}$$

where $\hbar$ is the reduced Planck constant, c is the speed of light in vacuum, and η_{det} is the detection efficiency, which is a function of the NA, the interference visibility, and the optical losses [22]. The working NA is fixed by the lenses used in the setup, which in our implementation are outside of the vacuum chamber; all the other relevant loss channels are independently measured. From these known losses, we calculate η_{det} to be 0.021(4). Including this value in Eq. (1), we predict the imprecision as a function of P, which agrees with our measured data, as shown in Fig. 3(d). For comparison, in the same figure, we plot both the ideal case, corresponding to $\eta_{\mathrm{det}} = 1$, and the imprecision of the forward technique extracted from our measurements.

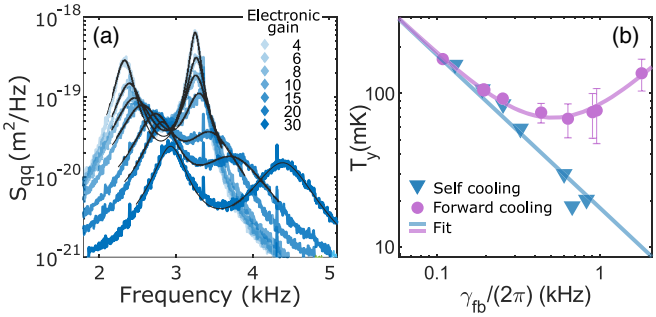

FIG. 4. Feedback cooling of the particle's radial motion. (a) Motional spectra acquired with self-homodyne detection for different electronic feedback gains. Black lines are fits to Lorentzians, used to determine the temperature and cooling rate for each of the two modes. (b) Temperature of the higher-frequency radial mode as a function of the cooling rate γ_{fb} obtained with the self-homodyne (blue diamonds) and forward-detection methods (purple circles). In the self-homodyne case, temperatures are fitted with $T_y = A/\gamma_{\mathrm{fb}}$, where $A = 112(7)$ rad K (blue line). In the forward-detection case, the temperature fit function includes the effect of measurement imprecision in the feedback loop [6].

The improved detection efficiency with respect to forward detection motivates us to harness the self-homodyne method for feedback cooling of the particle. We emphasize that this experiment was not designed to reach the ground state but rather as a proof-of-principle demonstration. The output of the self-homodyne detector is filtered and phase shifted in order to generate a feedback signal, which is applied to a set of electrodes in order to displace the particle. The field generated by the feedback electrodes has a projection along both radial axes of motion and thus cools both radial modes, at the cost of introducing a coupling between the modes due to the partial overlap of their spectral peaks. To ensure that the particle is cooled primarily via the self-homodyne signal, we reduce the gain of the feedback cooling based on forward detection by 37.8 dB in the radial plane; the forward feedback alone cools the particle to 200 K in this plane. Motion along $\hat{z}$ is not detected via self-homodyne, so we do not suppress cooling via forward detection along that axis. In Fig. 4(a), we plot self-homodyne spectra for different values of the feedback strength. As the feedback increases, the peak heights decrease due to the cooling force, and they shift to the right due to the spring force induced by the feedback. Because of the geometry of the feedback electrodes, the radial axes rotate in the xy plane as a function of the feedback strength [22]; we refer to the rotated axes as $\hat{x}'$ and $\hat{y}'$.

The temperatures $T_{y'}$ achieved along the rotated y' axis via feedback cooling are deduced by fitting the calibrated spectra with a Lorentzian and are plotted in Fig. 4(b) as a

function of the cooling rate γ_{fb}. For comparison, in the same figure, we plot T_y achieved with forward-detection feedback. Note that, in the case of forward-detection feedback, for which different electrodes are used, we observe neither a rotation of the radial axes nor a shift of the mode frequencies. We observe two distinct behaviors of the temperatures achieved with the two techniques: In the case of self-homodyne-based feedback, $T_{y'}$ is proportional to $\gamma_{\mathrm{fb}}^{-1}$, yielding a minimum measured temperature of 18(1) mK, where the uncertainty is due to both fit error and a bound on the coupling between the y' and x' modes. In the case of forward-detection feedback, T_y exhibits a minimum that arises from the balance between cooling strength and measurement noise introduced by the feedback loop. This minimum temperature is 3.8 times the one reached with self-homodyne. One would expect to reach even lower self-homodyne temperatures for higher values of γ_{fb} than those in Fig. 4(b), but the corresponding mode frequencies $\nu_{y'}$ lie outside the bandwidth of the feedback transfer function used for this experiment.

From a fit to the self-homodyne data and from the imprecision values determined from the calibrated spectra, we infer that the minimum temperature T_{min} should occur at $\gamma_{\mathrm{fb}} = 2\pi \times 31$ kHz, deep in the overdamped regime ($\gamma_{\mathrm{fb}} \gg \nu_{y'}$). In this regime, standard cold damping theory does not hold [32], and we cannot directly extrapolate T_{min}. It would be possible to extrapolate T_{min} if we were to increase the frequency $\nu_{y'}$, which could be done by choosing an appropriate feedback transfer function. This strategy has recently been used to cool the motion of a 10 kg mirror to nearly the quantum ground state [33].

In conclusion, we have realized self-homodyne detection of a nanoparticle's motion in a Paul trap and have demonstrated feedback cooling of that motion. The interferometric visibility between the nanoparticle and its image was measured to be 70%. By including a hemispherical mirror inside the vacuum chamber [34,35], we expect to obtain a visibility close to unity, and by increasing the NA to 0.35, we expect to reach the motional ground state ($\bar{n} < 1$), provided that measurement backaction is the main source of decoherence. We thus anticipate that the self-homodyne method will overcome the obstacle of limited optical access in Paul traps [6,36], as well as in hybrid traps [7,37] and magnetic traps [8–10]. Given the low intrinsic decoherence in these traps due to the lack of photon scattering, we expect that this detection approach will enable quantum experiments with macroscopic objects with a unique degree of isolation. As a final remark, the self-homodyne scheme can be used to measure q^2 if the mirror's position is locked to the minimum of the interference fringe in Fig. 1(b) [14]. It has been pointed out that, in an environment with sufficiently low decoherence, such a measurement would project a macroscopic wave function into a superposition state [38].

We thank Felix Tebbenjohanns and Martin Frimmer for discussions about the calibration technique and Simon Baier and Oriol Romero-Isart for their feedback on the manuscript. This work was supported by Austrian Science Fund (FWF) Project No. Y951, by the ESQ Discovery grant "Sympathetic detection and cooling of nanoparticles levitated in a Paul trap" of the Austrian Academy of Sciences, by the European Union's Horizon 2020 research and innovation program under the Marie Skłodowska-Curie Grant Agreement No. 801110, and by the Austrian Federal Ministry of Education, Science and Research (BMBWF). It reflects only the authors' view; the EU agency is not responsible for any use that may be made of the information it contains. G. A. thanks Wolfson College, Oxford for support.

*lorenzo.dania@uibk.ac.at

[1] L. Magrini, P. Rosenzweig, C. Bach, A. Deutschmann-Olek, S. G. Hofer, S. Hong, N. Kiesel, A. Kugi, and M. Aspelmeyer, Real-time optimal quantum control of mechanical motion at room temperature, Nature (London) **595**, 373 (2021).

[2] F. Tebbenjohanns, M. L. Mattana, M. Rossi, M. Frimmer, and L. Novotny, Quantum control of a nanoparticle optically levitated in cryogenic free space, Nature (London) **595**, 378 (2021).

[3] F. Tebbenjohanns, M. Frimmer, and L. Novotny, Optimal position detection of a dipolar scatterer in a focused field, Phys. Rev. A **100**, 043821 (2019).

[4] F. Gittes and C. F. Schmidt, Interference model for back-focal-plane displacement detection in optical tweezers, Opt. Lett. **23**, 7 (1998).

[5] U. Delić, M. Reisenbauer, K. Dare, D. Grass, V. Vuletić, N. Kiesel, and M. Aspelmeyer, Cooling of a levitated nanoparticle to the motional quantum ground state, Science **367**, 892 (2020).

[6] L. Dania, D. S. Bykov, M. Knoll, P. Mestres, and T. E. Northup, Optical and electrical feedback cooling of a silica nanoparticle levitated in a Paul trap, Phys. Rev. Research **3**, 013018 (2021).

[7] J. Millen, P. Z. G. Fonseca, T. Mavrogordatos, T. S. Monteiro, and P. F. Barker, Cavity Cooling a Single Charged Levitated Nanosphere, Phys. Rev. Lett. **114**, 123602 (2015).

[8] J. Gieseler, A. Kabcenell, E. Rosenfeld, J. D. Schaefer, A. Safira, M. J. A. Schuetz, C. Gonzalez-Ballestero, C. C. Rusconi, O. Romero-Isart, and M. D. Lukin, Single-Spin Magnetomechanics with Levitated Micromagnets, Phys. Rev. Lett. **124**, 163604 (2020).

[9] C. Timberlake, G. Gasbarri, A. Vinante, A. Setter, and H. Ulbricht, Acceleration sensing with magnetically levitated oscillators above a superconductor, Appl. Phys. Lett. **115**, 224101 (2019).

[10] B. R. Slezak, C. W. Lewandowski, J.-F. Hsu, and B. D'Urso, Cooling the motion of a silica microsphere in a magneto-gravitational trap in ultra-high vacuum, New J. Phys. **20**, 063028 (2018).

[11] V. Salakhutdinov, M. Sondermann, L. Carbone, E. Giacobino, A. Bramati, and G. Leuchs, Optical trapping of nanoparticles by full solid-angle focusing, Optica **3**, 1181 (2016).
[12] R. Maiwald, A. Golla, M. Fischer, M. Bader, S. Heugel, B. Chalopin, M. Sondermann, and G. Leuchs, Collecting more than half the fluorescence photons from a single ion, Phys. Rev. A **86**, 043431 (2012).
[13] C.-K. Chou, C. Auchter, J. Lilieholm, K. Smith, and B. Blinov, Note: Single ion imaging and fluorescence collection with a parabolic mirror trap, Rev. Sci. Instrum. **88**, 086101 (2017).
[14] G. Cerchiari, G. Araneda, L. Podhora, L. Slodička, Y. Colombe, and R. Blatt, Measuring Ion Oscillations at the Quantum Level with Fluorescence Light, Phys. Rev. Lett. **127**, 063603 (2021).
[15] G. Cerchiari, G. Araneda, L. Podhora, L. Slodička, Y. Colombe, and R. Blatt, Motion analysis of a trapped ion chain by single photon self-interference, Appl. Phys. Lett. **119**, 024003 (2021).
[16] A. K. Swan, L. A. Moiseev, C. R. Cantor, B. Davis, S. B. Ippolito, W. C. Karl, B. B. Goldberg, and M. S. Unlu, Toward nanometer-scale resolution in fluorescence microscopy using spectral self-interference, IEEE J. Sel. Top. Quantum Electron. **9**, 294 (2003).
[17] B. J. Davis, M. Dogan, B. B. Goldberg, W. C. Karl, M. S. Ünlü, and A. K. Swan, 4Pi spectral self-interference microscopy, J. Opt. Soc. Am. A **24**, 3762 (2007).
[18] B. Huang, M. Bates, and X. Zhuang, Super-resolution fluorescence microscopy, Annu. Rev. Biochem. **78**, 993 (2009).
[19] G. Cerchiari, L. Dania, D. S. Bykov, R. Blatt, and T. E. Northup, Position measurement of a dipolar scatterer via self-homodyne detection, Phys. Rev. A **104**, 053523 (2021).
[20] Interference between the scattered and reflected fields also occurs between the particle and the mirror; this region can be interpreted as one arm of an interferometer. However, extracting the information in this region would reduce the interference visibility in the first arm (at the detector).
[21] J. Eschner, C. Raab, F. Schmidt-Kaler, and R. Blatt, Light interference from single atoms and their mirror images, Nature (London) **413**, 495 (2001).
[22] See Supplemental Material at http://link.aps.org/supplemental/10.1103/PhysRevLett.129.013601 for more details on position calibration, power calibration, detection imprecision, micromotion minimization, feedback-induced axis rotation, radiation-pressure backaction, and fits to the feedback cooling data, which includes Refs. [23–26].
[23] F. Tebbenjohanns, M. Frimmer, A. Militaru, V. Jain, and L. Novotny, Cold Damping of an Optically Levitated Nanoparticle to Microkelvin Temperatures, Phys. Rev. Lett. **122**, 223601 (2019).
[24] D. J. Berkeland, J. D. Miller, J. C. Bergquist, W. M. Itano, and D. J. Wineland, Minimization of ion micromotion in a Paul trap, J. Appl. Phys. **83**, 5025 (1998).
[25] J. Keller, H. L. Partner, T. Burgermeister, and T. E. Mehlstäubler, Precise determination of micromotion for trapped-ion optical clocks, J. Appl. Phys. **118**, 104501 (2015).
[26] P. K. Ghosh, *Ion Traps* (Clarendon Press, Oxford, 1995).
[27] E. Hebestreit, M. Frimmer, R. Reimann, C. Dellago, F. Ricci, and L. Novotny, Calibration and energy measurement of optically levitated nanoparticle sensors, Rev. Sci. Instrum. **89**, 033111 (2018).
[28] Nanoparticles are manufactured by Bangs Laboratories, Inc.
[29] D. S. Bykov, P. Mestres, L. Dania, L. Schmöger, and T. E. Northup, Direct loading of nanoparticles under high vacuum into a Paul trap for levitodynamical experiments, Appl. Phys. Lett. **115**, 034101 (2019).
[30] A. A. Clerk, M. H. Devoret, S. M. Girvin, F. Marquardt, and R. J. Schoelkopf, Introduction to quantum noise, measurement, and amplification, Rev. Mod. Phys. **82**, 1155 (2010).
[31] J. D. Teufel, F. Lecocq, and R. W. Simmonds, Overwhelming Thermomechanical Motion with Microwave Radiation Pressure Shot Noise, Phys. Rev. Lett. **116**, 013602 (2016).
[32] C. Genes, D. Vitali, P. Tombesi, S. Gigan, and M. Aspelmeyer, Ground-state cooling of a micromechanical oscillator: Comparing cold damping and cavity-assisted cooling schemes, Phys. Rev. A **77**, 033804 (2008).
[33] C. Whittle *et al.*, Approaching the motional ground state of a 10-kg object, Science **372**, 1333 (2021).
[34] D. B. Higginbottom, G. T. Campbell, G. Araneda, F. Fang, Y. Colombe, B. C. Buchler, and P. K. Lam, Fabrication of ultrahigh-precision hemispherical mirrors for quantum-optics applications, Sci. Rep. **8**, 221 (2018).
[35] G. Araneda, G. Cerchiari, D. B. Higginbottom, P. C. Holz, K. Lakhmanskiy, P. Obšil, Y. Colombe, and R. Blatt, The Panopticon device: An integrated Paul-trap-hemispherical mirror system for quantum optics, Rev. Sci. Instrum. **91**, 113201 (2020).
[36] T. W. Penny, A. Pontin, and P. F. Barker, Performance and limits of feedback cooling methods for levitated oscillators: A direct comparison, Phys. Rev. A **104**, 023502 (2021).
[37] G. P. Conangla, R. A. Rica, and R. Quidant, Extending vacuum trapping to absorbing objects with hybrid Paul-optical traps, Nano Lett. **20**, 6018 (2020).
[38] O. Romero-Isart, A. C. Pflanzer, F. Blaser, R. Kaltenbaek, N. Kiesel, M. Aspelmeyer, and J. I. Cirac, Large Quantum Superpositions and Interference of Massive Nanometer-Sized Objects, Phys. Rev. Lett. **107**, 020405 (2011).